JHEP

Published for SISSA by Springer

Received: August 28, 2014
Revised: November 21, 2014
Accepted: November 23, 2014
Published: December 16, 2014

The not-so-sterile 4th neutrino: constraints on new gauge interactions from neutrino oscillation experiments

Joachim Kopp[a,b] **and Johannes Welter**[a]

[a] *Max Planck Institut für Kernphysik, Saupfercheckweg 1, 69117 Heidelberg, Germany*

[b] *PRISMA Cluster of Excellence and Mainz Institute for Theoretical Physics, Johannes Gutenberg University, 55099 Mainz, Germany*

E-mail: jkopp@uni-mainz.de, welter@mpi-hd.mpg.de

Abstract: Sterile neutrino models with new gauge interactions in the sterile sector are phenomenologically interesting since they can lead to novel effects in neutrino oscillation experiments, in cosmology and in dark matter detectors, possibly even explaining some of the observed anomalies in these experiments. Here, we use data from neutrino oscillation experiments, in particular from MiniBooNE, MINOS and solar neutrino experiments, to constrain such models. We focus in particular on the case where the sterile sector gauge boson A' couples also to Standard Model particles (for instance to the baryon number current) and thus induces a large Mikheyev-Smirnov-Wolfenstein potential. For eV-scale sterile neutrinos, we obtain strong constraints especially from MINOS, which restricts the strength of the new interaction to be less than ~ 10 times that of the Standard Model weak interaction unless active-sterile neutrino mixing is very small ($\sin^2\theta_{24} \lesssim 10^{-3}$). This rules out gauge forces large enough to affect short-baseline experiments like MiniBooNE and it imposes nontrivial constraints on signals from sterile neutrino scattering in dark matter experiments.

Keywords: Neutrino Physics, Beyond Standard Model

ArXiv ePrint: 1408.0289

doi:10.1007/JHEP12(2014)104

Contents

JHEP12(2014)104

1 Introduction and motivation

The possible existence of sterile neutrinos (Standard Model singlet fermions) with masses of order eV has been a widely discussed topic in astroparticle physics over the past few years. It is motivated by several anomalous results from short-baseline neutrino oscillation experiments, in particular the excesses of ν_e and $\bar{\nu}_e$ events in a ν_μ and $\bar{\nu}_\mu$ beam respectively observed by LSND [1] and MiniBooNE [2], the apparently lower than expected $\bar{\nu}_e$ flux from nuclear reactors [3–5] (see however [6]) and the deficit of ν_e in radioactive source experiments [7, 8]. Global fits [9–11, 11–15] show that these anomalies could be explained if sterile neutrinos with $\mathcal{O}(\text{eV})$ mass and $\mathcal{O}(10\%)$ mixing with ν_e and ν_μ exist. However, global fits also reveal that it is difficult to reconcile such a scenario with existing null results from other short-baseline oscillation experiments.

Constraints come also from cosmological observations, which slightly disfavor scenarios with extra relativistic degrees of freedom in the early Universe [16]. Cosmology also imposes a tight constraint on the sum of neutrino masses $\sum_j m_{\nu j} < 0.23$, where the sum runs over all neutrino mass eigenstates that are in thermal equilibrium in the early Universe. Note that these constraints would be relaxed if the recent BICEP-2 data on B-modes in the cosmic microwave background [17] is confirmed [18–22].

An interesting scenario that is unconstrained by cosmology is *self-interacting sterile neutrinos* [23, 24]. If interactions among sterile neutrinos are mediated by a scalar or gauge boson with a mass of order MeV or lighter, sterile neutrinos will feel a strong thermal potential in the early Universe which suppresses their mixing with active neutrinos and thus

prohibits their production through oscillations. Moreover, if the new interaction couples not only to sterile neutrinos, but also to dark matter, it has the potential to explain several problems with cosmic structure formation at small scales [24–26].

If a new interaction is shared between sterile neutrinos and ordinary matter (for instance in models with gauged baryon number coupled to sterile neutrinos and in scenarios in which a sterile sector gauge boson mixes kinetically with the photon), interesting signals in direct dark matter searches are possible [27–30]. The increased neutrino-nucleus scattering cross section might even explain some of the excess events observed by several experiments. On the other hand, such scenarios are more challenging for cosmology because of an additional sterile neutrino production mechanism through the gauge interaction. (Note that these constraints are still avoided for instance in scenarios with extra entropy production in the visible sector after sterile neutrino decoupling [31].)

In this paper, we investigate how novel interactions between sterile neutrinos and ordinary matter are constrained by neutrino oscillation experiments at short and long baseline. This topic has been discussed in a previous paper [32], the conclusions of which we will update below. For definiteness, we will focus on scenarios similar to the "baryonic sterile neutrino" scenario first introduced in [27], where the sterile neutrino couples to gauged baryon number (see also [33, 34] for anomaly-free models with gauges baryon number). We emphasize, however, that our results are directly applicable to any theory in which sterile neutrinos interact with Standard Model (SM) fermions through a new gauge force under which ordinary matter carries a net charge. (The last condition excludes models in which the coupling is only through kinetic mixing between the new gauge boson and the photon.) The new gauge current creates a Mikheyev-Smirnov-Wolfenstein (MSW) potential for sterile neutrinos propagating through ordinary matter and has thus a potentially large impact on neutrino oscillations. Since the mass of the new gauge boson in this model can be as low as 10 MeV (see [28] for detailed constraints) and since constraints on its coupling are weak [27], the strength of the effective interaction can be more than two orders of magnitude larger than the SM weak interactions responsible for the ordinary MSW effect. This implies that resonant enhancement of the oscillation amplitude could be relevant at $\mathcal{O}(\text{GeV})$ energies even for relatively large mass squared difference $\Delta m^2_{41} \sim \text{eV}$ between the mostly sterile and mostly active mass eigenstates. The model could thus potentially allow an explanation of some of the short-baseline oscillation anomalies with significantly smaller vacuum mixing angles than in sterile neutrino scenarios without new interactions.

The structure of the paper is as follows. In section 2, we briefly review models with new interactions in the sterile sector in general, and the "baryonic neutrino" model from [27] in particular. We map these models onto an effective field theory and discuss their implications for neutrino oscillations. In particular, we derive approximate analytical formulas for the oscillation probabilities. In section 3, we then present our main numerical results, which will set strong constraints on new forces coupling sterile neutrinos to SM particles. We will summarize and conclude in section 4.

JHEP12(2014)104

2 Models and formalism

2.1 New gauge bosons in the sterile neutrino sector

In the following we shortly describe the model proposed in [27, 28], originally introduced to study the impact of a new gauge force in the sterile neutrino sector on dark matter searches. The basic idea is to introduce a fourth left-handed neutrino flavour ν_b, sterile under SM interactions, which can have a relatively large coupling to baryons (10^2–10^3 times larger than the Fermi constant G_F) without being in conflict with current experimental bounds, like for examples constraints coming from meson decays such as $K \to \pi\bar{\nu}_b\nu_b$ [27]. It can be implemented by introducing a new $\mathrm{U}(1)_B$ gauge symmetry under which quarks have charge $g_b/3$ and the baryonic neutrino ν_b has charge g_b'. We will assume g_b and g_b' to be of order 0.1–1. To cancel anomalies, the introduction of additional fermions charged under $\mathrm{U}(1)_B$ will be necessary [33, 34], but we assume that these do not mix significantly with SM neutrinos and can be neglected. The baryonic gauge boson X acquires a mass when $\mathrm{U}(1)_B$ is broken by a new sterile sector Higgs field h_b. The relevant part of the Lagrangian after symmetry breaking can be written as [27]

$$\begin{aligned}\mathcal{L} \supset & -\frac{1}{4}F_{X,\mu\nu}F_X^{\mu\nu} + \frac{1}{2}m_X^2 X_\mu X^\mu \\ & + \bar{\nu}_b\gamma_\mu\left(i\partial^\mu + g_b' X^\mu\right)\nu_b + \sum_q \bar{q}\left(i\not{\partial}_{\mathrm{SM}} + \frac{1}{3}g_b\gamma_\mu X^\mu\right)q + \mathcal{L}_m\,, \end{aligned} \tag{2.1}$$

where q are the SM quark fields, $F_{X,\mu\nu} \equiv \partial_\mu X_\nu - \partial_\nu X_\mu$ is the field strength tensor of the baryonic vector boson X_μ and $m_X \sim 1\,\mathrm{GeV}$ is its mass. In a seesaw framework, the baryonic neutrino mixes with the SM through the terms

$$\mathcal{L}_m = -\sum_{\alpha,j} m_D^{\alpha j}\bar{\nu}_L^\alpha N_R^j - \sum_j m_b^j \bar{\nu}_{bL} N_R^j - \frac{1}{2}\sum_{i,j} m_R^{ij}\overline{\left(N_R^i\right)^C} N_R^j + h.c.\,, \tag{2.2}$$

with the Dirac mass matrix m_D of the active neutrinos ν_L^α, the Dirac mass vector of the baryonic neutrino m_b^j and the the Majorana mass matrix m_R^{ij} of the heavy right-handed neutrino fields N_R^j. The flavour index α runs over e, μ and τ, while the indices i and j run over all heavy right-handed neutrino states.

The Lagrangian of equation (2.1) implies the existence of a new MSW potential that sterile neutrinos experience while propagating in matter. This effect is caused by coherent elastic forward scattering on neutrons and protons and can lead to resonant enhancement of flavour oscillations. Since coherent forward scattering does not involve any momentum transfer, its amplitude can be most easily obtained from the low energy effective Lagrangian of baryonic neutral current interactions

$$\mathcal{L}_{b,\mathrm{eff}} = \frac{G_B}{2}\left[\bar{\nu}_b\gamma_\mu\left(1-\gamma_5\right)\nu_b\right]\left[\bar{p}\gamma^\mu p + \bar{n}\gamma^\mu n\right]. \tag{2.3}$$

Here, the effective coupling constant is $G_B \equiv g_b g_b'/m_X^2$. By treating neutrons and protons as a static background field [35], we obtain the matter potential for sterile neutrinos

$$V_b = G_B N_{\mathrm{nucl}}. \tag{2.4}$$

JHEP12(2014)104

The potential for sterile anti-neutrinos has opposite sign. Here, $N_{\rm nucl}$ is the number density of nucleons in the background matter. Note that G_B can be either positive or negative, depending on the relative sign of g_b and g'_b. In the following analysis we will use the ratio of the coupling constants

$$\epsilon \equiv \frac{G_B}{\sqrt{2}G_F} \tag{2.5}$$

as a measure for the relative strength of V_b compared to the potential $V_{\rm CC}$ that charged current (CC) interactions with electrons induce for electron neutrinos in the SM. The baryonic potential can be written as

$$V_b = V_{\rm CC} \cdot G_B/(\sqrt{2}G_F Y_e) = \epsilon\, V_{\rm CC}/Y_e \tag{2.6}$$

$$= \epsilon \cdot 7.56 \cdot 10^{-14}\ \text{eV} \cdot \left(\frac{\rho}{\text{g/cm}^3}\right), \tag{2.7}$$

where Y_e is the number of electrons per nucleon.

As mentioned in the introduction, baryonic sterile neutrinos could lead to novel signals in direct dark matter searches thanks to an enhanced sterile neutrino-nucleus scattering rate. Typically, observable effects in current experiments are expected if $\epsilon \gtrsim 100$ [27–30]. We will see in section 3.2 that such large values of ϵ are largely excluded for eV scale sterile neutrinos with substantial mixing into the active sector.

We wish to stress here that, while we use baryonic sterile neutrinos as a benchmark scenario, our results will apply to any scenario in which sterile neutrinos have new gauge interactions with SM fermions. It is important to keep in mind, though, that models with new forces in the lepton sector are much more tightly constrained than new baryonic interactions (see e.g. [28] for a review).

The mass terms in equation (2.2) lead to flavour mixing between ν_b and the active neutrinos, as can be seen by integrating out the heavy right-handed neutrinos and diagonalizing the resulting mass matrix. In this way, we obtain the 4×4 mixing matrix U connecting mass eigenstates $|\nu_i\rangle$ and flavour eigenstates $|\nu_\alpha\rangle$:

$$|\nu_\alpha\rangle = \sum_i U^*_{\alpha i}|\nu_i\rangle. \tag{2.8}$$

Since U is unitary, it can be parametrized by 6 rotation angles θ_{ij} and 3 complex phases δ_{ij}[1]

$$U \;=\; R_{34} \cdot R'_{24} \cdot R'_{14} \cdot R_{23} \cdot R'_{13} \cdot R_{12}. \tag{2.9}$$

Here, R_{ij} describes a rotation matrix in the ij plane, while R'_{ij} corresponds to a complex rotation by the angle θ_{ij} and phase δ_{ij}. Given the mixing matrix U and the mass squared difference Δm^2_{41} between the mostly sterile mass eigenstate ν_4 and the mostly active mass

[1] We omit the Majorana phases here since they do not contribute to neutrino flavour oscillations.

JHEP12(2014)104

eigenstate ν_1, one can write down the effective Hamiltonian[2] in flavour space:

$$H_{\text{eff}}^{\text{flavour}} = \frac{1}{2E} U \begin{pmatrix} 0 & & & \\ & \Delta m^2_{21} & & \\ & & \Delta m^2_{31} & \\ & & & \Delta m^2_{41} \end{pmatrix} U^\dagger + \begin{pmatrix} V_{\text{CC}} & & & \\ & 0 & & \\ & & 0 & \\ & & & V_b - V_{NC} \end{pmatrix}. \tag{2.10}$$

Here, $V_{NC} \equiv -\sqrt{2} G_F n_n/2$ is the contribution from SM neutral current interactions to the MSW potential. It is proportional to the number density n_n of neutrons in the background material.

The oscillation probability $P_{\nu_\alpha \to \nu_\beta}(t)$, i.e. the probability for a neutrino of initial flavour α to be converted into flavour β after traveling a time t, can then be obtained by diagonalizing the effective Hamiltonian according to $H_{\text{eff}}^{\text{flavour}} = \tilde{U} \text{diag}(\lambda_1, \lambda_2, \lambda_3, \lambda_4) \tilde{U}^\dagger$ and inserting the eigenvalues λ_i and the effective mixing matrix $\tilde{U}$ into the well-known formula

$$P_{\nu_\alpha \to \nu_\beta} = \left| \langle \nu_\beta | \nu_\alpha(t) \rangle \right|^2 = \left| \sum_j \tilde{U}^*_{\alpha j} \tilde{U}_{\beta j} e^{-i \lambda_j L} \right|^2. \tag{2.11}$$

2.2 Approximate oscillation probabilities

As a prelude to the numerical fits we are going to present in section 3, we give here approximate analytic expressions for the oscillation probabilities in the baryonic sterile neutrino model and in models with new sterile neutrino-SM interactions in general. Similar calculations have been carried out previously in [32] and we will compare these results to ours in section 2.3.

Our starting point is to assume $|\Delta m^2_{41}| \gg |\Delta m^2_{31}|, \Delta m^2_{21}$, which is a good approximation at sufficiently short baselines. Moreover, we neglect the SM MSW potentials V_{NC} (arising from Z exchange diagrams) and V_{CC} (arising from W exchange diagrams) against the baryonic potential V_b, which we assume to be much larger. With these approximations, mixing among the three active flavour eigenstates becomes irrelevant. (They can, however, still oscillate into each other through their mixing with ν_b.) We also set $U_{\tau 4} = 0$ for simplicity, following [32]. With these assumptions, diagonalization of the Hamiltonian $H_{\text{eff}}^{\text{flavour}}$ from equation (2.10) yields for the eigenvalues λ_i

$$\lambda_1 = \lambda_2 = 0, \qquad \lambda_3 = \frac{1}{2}\Big(V_b + \frac{\Delta m^2_{41}}{2E} - A\Big), \qquad \lambda_4 = \frac{1}{2}\Big(V_b + \frac{\Delta m^2_{41}}{2E} + A\Big). \tag{2.12}$$

The elements of the unitary matrix $\tilde{U}$ are

$$\begin{aligned} &\tilde{U}_{\mu 1} = \tilde{U}_{e1} = 0, \qquad |\tilde{U}_{e2}|^2 = \frac{|U_{\mu 4}|^2}{1 - |U_{s4}|^2}, \quad |\tilde{U}_{\mu 2}|^2 = \frac{|U_{e4}|^2}{1 - |U_{s4}|^2}, \\ &|\tilde{U}_{e4}|^2 = |U_{e4}|^2 \frac{\frac{\Delta m^2_{41}}{2E}\Big[A + \frac{\Delta m^2_{41}}{2E} - V_b\Big]}{A\Big[A + \frac{\Delta m^2_{41}}{2E} + V_b\Big]}, \qquad |\tilde{U}_{\mu 4}|^2 = |U_{\mu 4}|^2 \frac{\frac{\Delta m^2_{41}}{2E}\Big[A + \frac{\Delta m^2_{41}}{2E} - V_b\Big]}{A\Big[A + \frac{\Delta m^2_{41}}{2E} + V_b\Big]}. \end{aligned} \tag{2.13}$$

[2] *Effective* means that terms proportional to the unit matrix are omitted because they do not contribute to flavour oscillations. Also note that we assume a definite three-momentum that is the same for all contributing mass eigenstates so that one can approximate $E_i \approx |\mathbf{p}| + m_i^2/(2E)$. It is well-known that this approximation, though technically unjustified, leads to correct results for neutrino oscillation probabilities [36].

JHEP12(2014)104

Here, we have introduced the abbreviation

$$A = |V_b| \cdot \sqrt{1 + (4|U_{s4}|^2 - 2)\,\frac{\Delta m^2_{41}}{2EV_b} + \left(\frac{\Delta m^2_{41}}{2EV_b}\right)^2}. \tag{2.14}$$

With these formulas at hand and using the unitarity condition $\sum_i \tilde{U}^*_{\alpha i}\tilde{U}_{\alpha i} = 1$ as well as the observation that $\tilde{U}_{\mu 2}\tilde{U}^*_{e2}\tilde{U}^*_{\mu 4}\tilde{U}_{e4}$ is real, it is straightforward to calculate the oscillation probabilities according to equation (2.11). For $\alpha = \mu$ and $\beta = \mu, e$ we obtain

$$\begin{aligned} P_{\nu_\mu\to\nu_e} &= -4\frac{|U_{e4}|^2|U_{\mu4}|^2|U_{s4}|^2}{1-|U_{s4}|^2}\left(\frac{\Delta m^2_{41}}{2EA}\right)^2 \sin^2\phi_1 + 2\frac{|U_{e4}|^2|U_{\mu4}|^2}{(1-|U_{s4}|^2)^2}\left(1+\frac{V_b - V_{\rm res}}{A}\right)\sin^2\phi_2 \\ &\quad +2\frac{|U_{e4}|^2|U_{\mu4}|^2}{(1-|U_{s4}|^2)^2}\left(1-\frac{V_b - V_{\rm res}}{A}\right)\sin^2\phi_3, \end{aligned} \tag{2.15}$$

$$P_{\nu_\mu\to\nu_b} = 4|U_{\mu4}|^2|U_{s4}|^2\left(\frac{\Delta m^2_{41}}{2EA}\right)^2 \sin^2\phi_1, \tag{2.16}$$

$$P_{\nu_\mu\to\nu_\mu} = 1 - P_{\nu_\mu\to\nu_e} - P_{\nu_\mu\to\nu_b}, \tag{2.17}$$

where the oscillation phases are

$$\phi_1 = \frac{\lambda_4 - \lambda_3}{2}L = \frac{L}{2}A, \tag{2.18}$$

$$\phi_2 = \frac{\lambda_3}{2}L \qquad = \frac{L}{4}\left(V_b + \frac{\Delta m^2_{41}}{2E} - A\right), \tag{2.19}$$

$$\phi_3 = \frac{\lambda_4}{2}L \qquad = \frac{L}{4}\left(V_b + \frac{\Delta m^2_{41}}{2E} + A\right) \tag{2.20}$$

and $V_{\rm res}$ is the value of the matter potential at which A takes its minimal value $|U_{s4}|\sqrt{1-|U_{s4}|^2}\,\Delta m^2_{41}/E$. It is given by

$$V_{\rm res} = -\frac{\Delta m^2_{41}}{2E}\left(2|U_{s4}|^2 - 1\right) \tag{2.21}$$

and corresponds to the new MSW resonance condition. Whether the resonance is in the neutrino or anti-neutrino sector depends on the sign of V_b, i.e. the relative sign of the charges g_b and g'_b. With the assumption $\sin^2\theta_{24} < 0.5$ and for $V_b < 0$ ($V_b > 0$) the resonance condition can be fulfilled only in the neutrino (anti-neutrino) sector. For $\Delta m^2_{41} = 1\,\mathrm{eV}^2$, a matter density of 3 g/cm^3 and a neutrino energy of 1 GeV, the resonance condition is fulfilled for neutrinos if $\epsilon = G_B/\sqrt{2}G_F \simeq -2\times 10^3$ and for anti-neutrinos if ϵ has opposite sign. For oscillation experiments, we see that matter enhancement of active-to-sterile neutrino oscillations is expected predominantly in high energy ($\mathcal{O}$(GeV)) experiments and only if the new gauge force is several orders of magnitude stronger than SM weak interactions. For weaker gauge forces, the new resonance moves to higher energies that are only accessible with atmospheric or cosmic neutrinos.

Note that equation (2.21) has a structure similar to the expression for the standard MSW resonance condition. To see this, consider the matrix element $|U_{s4}|^2$ in the parametrization of equation (2.9): $|U_{s4}|^2 = \cos^2\theta_{14}\cos^2\theta_{24}\cos^2\theta_{34}$. If $\cos^2\theta_{34}$,

JHEP12(2014)104

$\cos^2\theta_{14} \approx 1$, we have $V_{\rm res} = -(\Delta m^2_{41}/2E)\cos 2\theta_{24}$. However, unless $\Delta m^2_{41}/2E$ is much larger than V_b, oscillations at short baseline cannot be approximately described in an effective two-flavour framework, unlike the 3+1 model without non-standard matter effects. The reason is that, without the extra matter term, three eigenvalues of the Hamiltonian can be set to zero at short baseline, while large V_b implies that this is only possible for two of them.

On the other hand, in the limit of very large matter potential, $V_b \gg \Delta m^2_{41}/(2E)$, the term proportional to $\sin^2\phi_2$ in equation (2.15) dominates over the terms containing $\sin^2\phi_1$ and $\sin^2\phi_3$ since the latter two are of higher order in $\Delta m^2_{41}/(2EV_b)$. If we furthermore assume the baseline is not too long, in particular $(\Delta m^2_{41})^2/(4E^2V_b)\cdot L/2 \ll 1$, we can approximate $\phi_2 \approx (L/2)(1-|U_{s4}|^2)\Delta m^2_{41}/(2E)$ and obtain for the oscillation probability of equation (2.15) the effective two-flavour formula

$$P_{\nu_\mu\to\nu_e} \approx 4\frac{|U_{e4}|^2|U_{\mu4}|^2}{\left(1-|U_{s4}|^2\right)^2}\cdot\sin^2\left(\frac{L}{2}\left(1-|U_{s4}|^2\right)\frac{\Delta m^2_{41}}{2E}\right) + \mathcal{O}\left(\left(\frac{\Delta m^2_{41}}{2EV_b}\right)^2\right). \quad (2.22)$$

As expected, in the limit of large matter potential V_b, the corresponding neutrino ν_b decouples from flavour oscillations, $P_{\nu_\mu\to\nu_b} \approx 0$ and the ν_μ survival probability becomes $P_{\nu_\mu\to\nu_\mu} \approx 1 - P_{\nu_\mu\to\nu_e}$.

We do not expect that scenarios with large V_b can explain the short-baseline anomalies better than conventional models without new interactions. The reactor [3–5] and gallium [7, 8] experiments were too low in energy; in LSND [1], neutrinos traveled mostly through air; MiniBooNE could in principle be sensitive to new matter effects, but resonant enhancement could only explain an anomaly in either the neutrino or the anti-neutrino sector, while the data shows similar deviations from expectations in both sectors.[3] On the other hand, we expect that MiniBooNE — along with long-baseline experiments like MINOS and with solar neutrinos — will impose tight constraints on V_b.

2.3 Accuracy of analytic approximations

In the following, we discuss the implications of sterile neutrinos with non-standard matter effects in terrestrial long-baseline experiments, taking MiniBooNE and MINOS as examples. In doing so, we also compare our analytic expressions (2.17) and (2.15) to a numerical computation in the full four flavour framework and to the results of [32].

To obtain the exact four-flavour oscillation probabilities, we diagonalize the effective Hamiltonian of equation (2.10) numerically and use the resulting eigenvalues and eigenvectors in equation (2.11). In doing so, we absorb the neutral current potential $V_{\rm NC}$ into a redefinition of V_b.[4] To average out fast oscillations that would not be resolvable by experiments, we also implement a low-pass filter by multiplying each term in the oscillation

[3] Note that in earlier MiniBooNE data [37–39], there appeared to be mild tension between the neutrino and anti-neutrino mode data. This motivated the authors of [32] to consider resonantly enhanced active-sterile neutrino mixing even as a possible *explanation* of the MiniBooNE anomaly.

[4] This is only approximately correct if $V_b \simeq V_{\rm NC}$ and the proton-to-neutron ratio is varying along the neutrino trajectory. Since we are mainly interested in scenarios with $V_b \gg V_{\rm NC}$, our results are insensitive to this subtlety.

JHEP12(2014)104

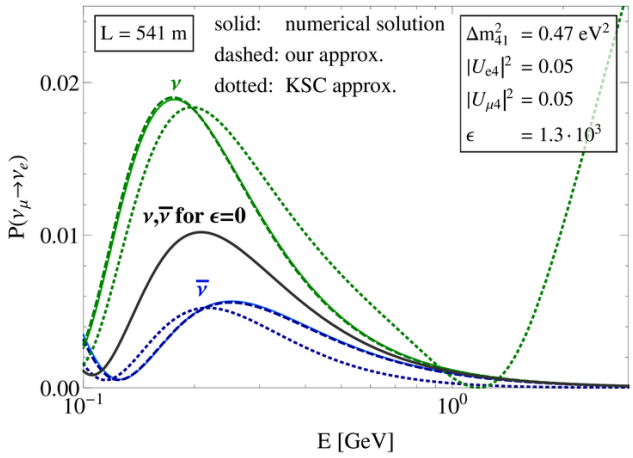

Figure 1. The electron neutrino (green) and anti-neutrino (blue) appearance probability in a model with a large MSW potential in the sterile sector (for instance the baryonic sterile neutrino model from [27]). We use the baseline $L = 541$ m and the energy range 0.1–3 GeV of the MiniBooNE experiment and take the favored model parameters from [32]: $\epsilon = G_B/(\sqrt{2}G_F) = 882$ ($\Leftrightarrow V_b = 2 \cdot 10^{-10}$ eV for $\rho = 3$ g/cm^3), $\Delta m^2_{41} = 0.47\,\mathrm{eV}^2$, $|U_{s4}|^2 = 0.9$, $|U_{e4}|^2 = |U_{\mu 4}|^2 = 0.05$. (We will see below, that this particular parameter point is in fact excluded by MINOS data, though.) For the standard oscillation parameters, we have used the results of the global fit "Free Fluxes and RSBL" of [42]. In black, we show also the prediction of a sterile neutrino model without new interactions ($\epsilon = 0$). Dashed lines correspond to our analytic approximations, which coincide with numerical results (solid curves) in this baseline and energy range, while dotted lines show the results from [32].

probability equation (2.11) by a Gaussian factor [40]. This yields:

$$P_{\nu_\alpha \to \nu_\beta} = \sum_{j,k} \tilde{U}^*_{\alpha j} \tilde{U}_{\beta j} \tilde{U}_{\alpha k} \tilde{U}^*_{\beta k} \exp\left[-iL(\lambda_j - \lambda_k)\right] \exp\left[-L^2(\lambda_j - \lambda_k)^2 \cdot \frac{\sigma_f(E)^2}{2E^2}\right], \quad (2.23)$$

where $\sigma_f(E)$ is the energy width of the filter, which is related to the energy resolution of the experiment. This form for the low-pass filter can also be motivated in a wave packet treatment, where the finite energy resolution of the production and detection processes determines the width of the neutrino wave packets (see [41] and references therein). When comparing analytical and numerical results, we also apply such a low-pass filter to the analytic expressions (2.15) and (2.17) by replacing the oscillation terms $\sin^2\phi_i$ according to

$$\sin^2\phi_i \mapsto \frac{1}{2}\left(1 - \cos(2\phi_i) \cdot \exp\left[-(2\phi_i)^2 \frac{\sigma_f(E)^2}{2E^2}\right]\right). \quad (2.24)$$

In the following, we choose $\sigma_f(E) = 0.01$ GeV.

In the calculation of the analytical formulas in [32] the eigenvalues λ_i are approximated by setting $A \approx V_b + \frac{\Delta m^2_{41}}{2E}$ (i.e. taking $|U_{s4}| = 1$ in equation (2.14)). This leads to $\lambda_1 = \lambda_2 = \lambda_3 = 0$ and $\lambda_4 = V_b + \Delta m^2_{41}/2E$. The oscillation phases of equations (2.18)–(2.20) then become $\phi_1 = \phi_3 = \frac{1}{2}L(V_b + \Delta m^2_{41}/2E)$ and $\phi_2 = 0$. With this replacements our equation (2.15) reduces to equations (21)–(22) in [32]. In the limit of large V_b we see from equation (2.22) that this approximation is only valid if $L/2(1 - |U_{s4}|^2)\Delta m^2_{41}/(2E) \ll 1$.

JHEP12(2014)104

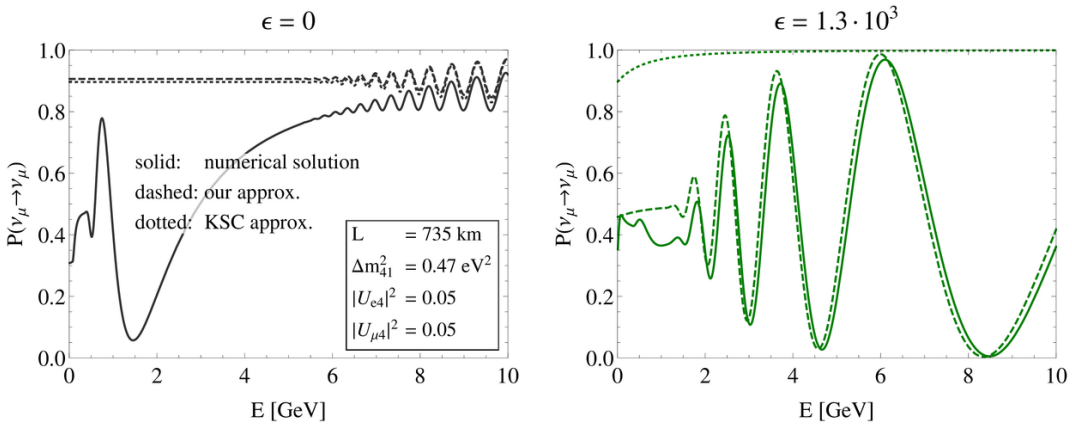

Figure 2. We show the survival probability $P_{\nu_\mu \to \nu_\mu}$ for the MINOS baseline of $L = 735\,\text{km}$ and energies up to 10 GeV for $\epsilon = 0$ (left panel) and $\epsilon = 882$ ($\Leftrightarrow V_b = 2 \cdot 10^{-10}\,\text{eV}$ for $\rho = 3\,\text{g/cm}^3$) (right panel) using the best fit parameters from the LSND/MiniBooNE fit of [32]. Solid curves correspond to a numerical calculation in the full four flavour oscillation framework, using for the standard oscillation parameters the values from the fit "Free Fluxes and RSBL" of [42]. Dashed curves show our analytic approximation, equation (2.17), while dotted curves correspond to equations 20 and 28 of [32]. The comparison shows that, when the new matter potential V_b is switched on ($\epsilon > 0$), the active-sterile oscillation mode dominates over the standard atmospheric oscillation pattern, an effect which is not captured by the approximations made in [32].

Since the latter condition is fulfilled in the L/E regime at which the LSND and MiniBooNE experiments are sensitive to $\nu_\mu \to \nu_e$ flavour transitions, the approximation from [32] is applicable there. This can be seen in figure 1, where the transition probabilities for neutrinos (in green) and anti-neutrinos (in blue) are shown for $L = 541$ m and $E = 0.1$–$3\,\text{MeV}$. We have taken the model parameters at the best fit point from [32] (which we will show to be in fact excluded by MINOS in section 3.2). Dashed curves correspond to our analytical approximation (equation (2.15)), which agrees extremely well with numerical results, while dotted curves show the approximation from equations (21)–(22) of [32]. The difference between the neutrino and anti-neutrino sectors originates from the different signs of the matter potential. As expected, $\epsilon > 0$ ($\Leftrightarrow V_b > 0$) leads to a resonant enhancement of the anti-neutrino transition probabilities and a suppression of the neutrino transition probabilities compared to the case $\epsilon = 0$ (black curve). We see that the approximations used in [32] are fairly accurate in the most relevant energy range below 1 GeV, but fail at higher energies.

Since standard and non-standard matter effects are most relevant at long baseline ($\gtrsim$ few $\times$ 100 km), it is important to also study the disappearance probability $1 - P_{\nu_\mu \to \nu_\mu}$ as a function of energy for long-baseline oscillation experiments like MINOS. MINOS has measured $P_{\nu_\mu \to \nu_\mu}$ at a baseline of $L = 735$ km in the energy range 1–50 GeV. The oscillation probabilities for this baseline and energy range are shown in figure 2 for $\epsilon > 0$ (right panel) and also for the Standard Model ($\epsilon = 0$, left panel). We see that, due to matter-enhanced oscillations inside the earth, a scenario with strong non-standard matter effects leads to

JHEP12(2014)104

very large muon disappearance even at energies as high as 10 GeV, well above the standard oscillation maximum at ~ 1.5 GeV. This is in conflict with MINOS data and we therefore expect that MINOS is able to place very strong constraints on new matter effects in the sterile neutrino sector. Figure 2 also implies that the parameters favored in [32] are ruled out by MINOS.

Comparing numerical results (solid lines) to our analytic approximation (dashed lines), we find, as expected, that the approximations of equations (2.15) and (2.17) are accurate at $\Delta m^2_{31} L/(2E) \sim 1$ only if V_b is very large. We also see that the analytic approximations from [32] (dotted curves in figure 2) are not applicable at long baseline even for large V_b. For example, in the MINOS case, $\Delta m^2_{41} L/(2E) \cdot \text{eV}^2 \sim 100$ for $\Delta m^2_{41} \sim \text{eV}^2$, the phase ϕ_2 (see equations (2.19) and (2.22)) becomes non-negligible. This is the reason why our conclusions regarding the importance of MINOS data for constraining sterile neutrino matter effects differ from those of [32], where ϕ_2 has been neglected.

3 Constraints from oscillation experiments

From the analysis in the previous section we expect that the baryonic sterile neutrino model (or models with new sterile neutrino-SM interactions in general) could potentially explain by resonant enhancement an event excess in the MiniBooNE neutrino or anti-neutrino data (but not in both), but is strongly constrained by data from long-baseline experiments. Therefore, we now derive limits on the model using a numerical χ^2 analysis of data from MiniBooNE, MINOS and also solar neutrino experiments.

3.1 Analysis method

In our analysis we fix the standard oscillation parameters at their best fit values from the global fit by Gonzalez-Garcia et al. [42] (see table 1) and we assume a normal mass ordering. We have checked that our results for inverted ordering are very similar, with only the solar limits becoming somewhat weaker. (We will comment on this in more detail in section 3.2.) For simplicity we set $\delta_{13} = \delta_{14} = \delta_{24} = 0$ because none of the experiments considered here is sensitive to CP violation in the small V_b limit and equations (2.15)–(2.17) show that also the leading terms in the oscillation probabilities for large V_b are independent of complex phases. We fix the mixing angle $\theta_{34} = 0$ since MiniBooNE is not sensitive to this angle and MINOS has only very limited sensitivity [15]. The impact of $\theta_{34} > 0$ on the constraints from solar experiments will be discussed in section 3.2. Finally, we set $\sin^2 2\theta_{14} = 0.12$ so that the reactor anomaly [3–5] can be explained. We will comment on the effect of relaxing this assumption also in section 3.2. The constraints we impose on the parameter space are also summarized in table 1. The remaining three parameters $\epsilon = G_B/(\sqrt{2}G_F)$, Δm^2_{41} and θ_{24} are scanned over the ranges $|\epsilon| = 1 - 32000$, $\Delta m^2_{41}/eV^2 = 0.01 - 11$ and $\sin^2\theta_{24} = 0.0001 - 1$.

We now discuss the details of our fits to MINOS, MiniBooNE and solar neutrino data.

JHEP12(2014)104

$\sin^2\theta_{12}$	$\sin^2\theta_{23}$	$\sin^2\theta_{13}$	Δm^2_{21} [eV^2]	Δm^2_{31} [eV^2]	δ_{13}, δ_{14} δ_{24}	$\sin^2 2\theta_{14}$	$\sin^2\theta_{34}$
0.302	0.413	0.0227	$7.5 \cdot 10^{-5}$	$2.473 \cdot 10^{-3}$	0	0.12	0

Table 1. The parameter values of the baryonic sterile neutrino model that we have fixed in our parameter scan.

3.1.1 MINOS

For MINOS, we use GLoBES [43, 44] to compute the energy dependent oscillation probabilities $P_{\rm near}(E)$ for the near detector and $P_{\rm far}(E)$ for the far detector numerically. We include a low pass filter according to equation (2.23) with $\sigma_f(E) = 0.06 \cdot E$. The matter density ρ along the neutrino trajectory to the far detector is assumed to be constant at its average value

$$\langle \rho_{\rm far} \rangle = \frac{2}{L_{\rm far}} \int_{\sqrt{R_\oplus^2 - (L_{\rm far}/2)^2}}^{R_\oplus} \rho(r) \frac{d}{dr} \left(\sqrt{r^2 - R_\oplus^2 + (L_{\rm far}/2)^2} \right) dr. \tag{3.1}$$

In this expression, which can be understood from geometric arguments, r is the distance of the neutrino from the center of the earth, $R_\oplus$ is the radius of the earth and $L_{\rm far} = 735\,{\rm km}$ is the neutrino path length from the source to the far detector [45]. Using the matter density profile from the Preliminary Reference Earth Model (PREM) [46] we obtain $\langle \rho_{\rm far} \rangle \approx 2.36\,{\rm g/cm^3}$.

For large V_b, matter effects can be relevant even in the near detector at a baseline $L_{\rm target} = 965\,{\rm m}$ from the target. In computing the average matter density $\langle \rho \rangle_{\rm near}$ that neutrinos experience on their way to the near detector, we account for the fact that they first travel along the evacuated decay pipe with a length of $L_{\rm pipe} = 675\,{\rm m}$. We estimate $\langle \rho \rangle_{\rm near} \approx (L_{\rm target} - L_{\rm pipe})/L_{\rm near} \cdot 3 \frac{\rm g}{\rm cm^3}$, where $L_{\rm near} \simeq 763\,{\rm m}$ is the average distance between the neutrino production vertex and the near detector. It is obtained from the decay length of the neutrinos' parent pions, which have an average energy of $4 - 5\,{\rm GeV}$ [47].

We compute the theoretically predicted event spectrum $N_{\rm osc}$ by multiplying the ratio $P_{\rm far}(E)/P_{\rm near}(E)$ with the background-subtracted prediction for the MINOS event rate in the absence of oscillations, $N_{\text{no osc}}$:

$$N_{\rm osc}(E) = \left[N_{\text{no osc}}(E) - N_{\rm bg}(E) \right] \frac{P_{\rm far}(E)}{P_{\rm near}(E)}. \tag{3.2}$$

The no-oscllation rate $N_{\text{no osc}}(E)$ and the background rate $N_{\rm bg}(E)$ are taken from [48], which is similar to [49] but contains data up to 50 GeV. The higher energy data is important to us since it increases the sensitivity at low matter potential V_b.

To account for the finite energy resolution of the detector, we fold $N_{\rm osc}$ with the detector response function $f(E, E')$, which maps the true event energy E' to the reconstructed energy E. Finally, we also add the small experimental background $N_{\rm bg}(E)$:

$$N_{\rm th}(E) = N_{\rm bg}(E) + \int f(E, E') N_{\rm osc}(E') dE'. \tag{3.3}$$

We assume a Gaussian shape for $f(E, E')$,

$$f(E, E') = \frac{1}{\sigma(E')\sqrt{2\pi}} \exp\left(-\frac{(E - E')^2}{2\sigma^2(E')} \right), \tag{3.4}$$

JHEP12(2014)104

where we choose $\sigma(E') = 0.2\,\mathrm{GeV}\sqrt{E'/\mathrm{GeV}}$. This choice allows us to reproduce the oscillated event rates and the constraints on θ_{23} and Δm^2_{31} from [49] with good accuracy. When evaluating equation (3.3) numerically, we discretize the integral so that $N_{\mathrm{osc}}(E)$ needs to be evaluated only at fixed support points E'_j with a step size of $\Delta E'_j = 0.25\,\mathrm{GeV}$ in between. (We have checked that choosing a smaller value for $\Delta E'_j$ does not change our results significantly, which implies that possible aliasing effects are under control.) Following the MINOS analysis [48], events are binned for the analysis according to their reconstructed energy E. The rate in th i-th bin is given by

$$N^i_{\mathrm{th}} = \int_{E_i-\Delta E_i/2}^{E_i+\Delta E_i/2} N_{\mathrm{th}}(E)\,dE = N^i_{\mathrm{bg}} + \sum_j F^{ij} N_{\mathrm{osc}}(E'_j), \tag{3.5}$$

where N^i_{bg} is the total background in the i-th bin and the elements of the detector response matrix F^{ij} are $F^{ij} \equiv= \int_{E_i-\Delta E_i/2}^{E_i+\Delta E_i/2} f(E, E'_j)\,dE$. It is important to note that the F^{ij} need to be computed only once.

From equation (3.5) we compute χ^2 according to

$$\chi^2 = \sum_i \left(\frac{N^i_{\mathrm{th}} - N^i_{\mathrm{exp}}}{\sqrt{N^i_{\mathrm{exp}}} + 0.1 \cdot N^i_{\mathrm{exp}}} \right)^2, \tag{3.6}$$

where N^i_{exp} is the observed event rate in the i-th energy bin [48] and the sum runs over all energy bins. Note that we have included an additional uncertainty of 10% in order to account for systematic errors without modeling them in detail. Like our choice of $\sigma(E')$ in equation (3.4), also our simplified treatment of systematic errors has been confirmed by cross-checking our simulations against the results of [15, 49].

In figure 3, we compare our prediction for the oscillated neutrino spectrum in MINOS assuming standard 3-flavour oscillations (blue shaded histogram) to the official MINOS prediction (blue unshaded histogram) and to the data (black points with error bars). We find excellent agreement, which validates our calculations. We also show the MINOS no oscillation prediction (red histogram) which is the starting point for our predictions, as well as the survival probability $P_{\nu_\mu \to \nu_\mu}$ (dashed green line; corresponding vertical scale shown on the right).

3.1.2 MiniBooNE

As for MINOS, the oscillation probabilities for MiniBooNE are calculated numerically in the full four flavour framework with the help of GLoBES [43, 44], including a low pass filter according to equation (2.23) with $\sigma_f(E) = 0.06E$. Since the MiniBooNE decay pipe is only 50 m long, while the distance from the target to the detector is $L = 541$ m, we neglect the effect of the finite pion decay length. Instead, we take the matter density to be $\langle\rho\rangle \sim 3\,\mathrm{g/cm^3}$ along the whole neutrino trajectory.

We use a χ^2 analysis to compare our predicted oscillation probabilities with the experimentally measured probabilities, which are given in [50] as a function of L/E. The data from [50] are shown in figure 4 together with the trivial no-oscillation prediction and with

JHEP12(2014)104

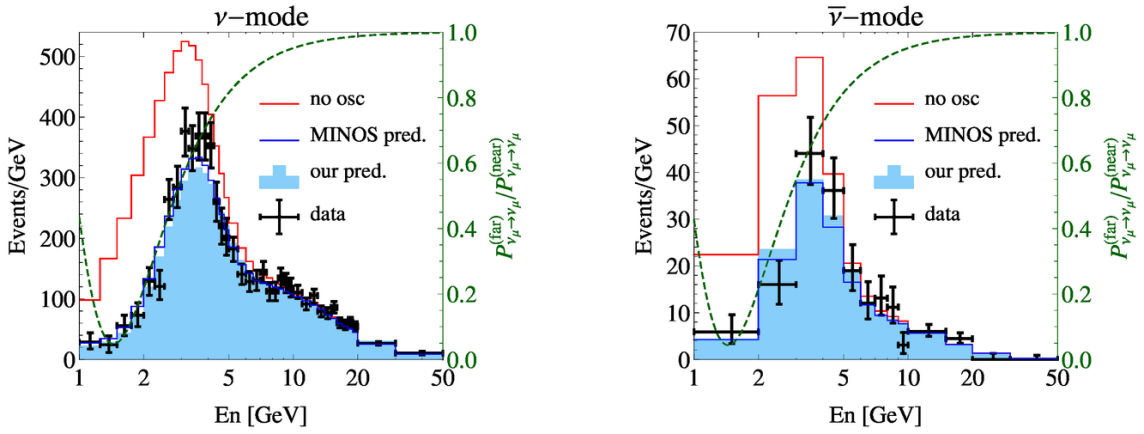

Figure 3. The measured and predicted event spectra for the MINOS ν_μ (left) and $\overline{\nu}_\mu$ (right) disappearance measurements. The red histogram is the MINOS prediction assuming no neutrino oscillation [48]. In blue, we show the predicted event spectrum including oscillations according to equation (3.3), assuming standard three flavour oscillations with the parameters listed in table 1. The blue shaded histogram is our prediction, the unshaded histogram is the prediction by the MINOS collaboration. We overlay the survival probability $P_{\nu_\mu\to\nu_\mu}$ (dashed green curve and vertical scale on the right).

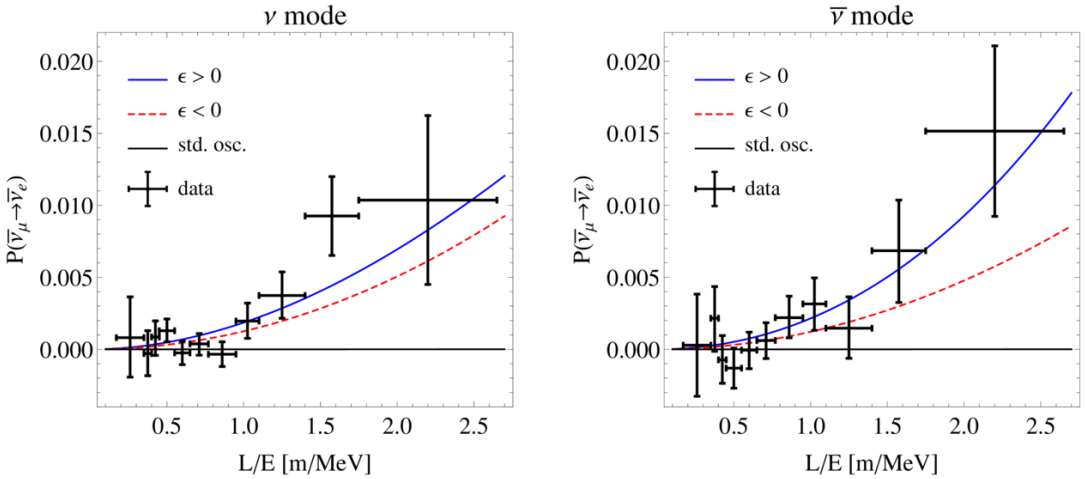

Figure 4. The measured MiniBooNE $\nu_\mu \to \nu_e$ (left) and $\bar{\nu}_\mu \to \bar{\nu}_e$ (right) appearance probabilities compared to the predictions of the baryonic sterile neutrino scenario for $\epsilon > 0$ (blue line) and $\epsilon < 0$ (dashed red line) at the MiniBooNE best fit points from table 2. Without sterile neutrinos, the appearance probability at the MiniBooNE baseline is approximately zero (solid black line).

our prediction for the MiniBooNE best fit points in the baryonic sterile neutrino scenario for $\epsilon > 0$ and $\epsilon < 0$.

JHEP12(2014)104

3.1.3 Solar neutrinos

We analyze solar neutrino oscillation data by comparing the measured ν_e survival probability $P_{\nu_e \to \nu_e}$ at different energies to our theoretical predictions. The data points are taken from [51] and include results from Super-Kamiokande, SNO, Borexino and radiochemical experiments on CC ν_e interactions. We do not include SNO NC data in our analysis because even for $\epsilon \sim 10^2$, the cross section for A'-mediated NC scattering is still smaller than the cross section for Z-mediated NC scattering in the SM. This is related to the axial vector structure and the isospin-dependent nature of Z boson couplings, compared to the vector structure and isospin-independent nature of A' couplings [27].

In calculating $P_{\nu_e \to \nu_e}$, we assume MSW flavour transitions to be fully adiabatic and we account for the fact that solar neutrinos arrive at the earth as an incoherent mixture of mass eigenstates. We obtain $P_{\nu_e \to \nu_e}$ according to

$$P_{\nu_e \to \nu_e} = \sum_i |U_{ei}|^2 \cdot |\tilde{U}_{ei}(0)|^2, \tag{3.7}$$

where $\tilde{U}_{ei}(0)$ is the mixing matrix in matter at the center of the Sun ($t = 0$) and U_{ei} is the vacuum mixing matrix. We neglect earth matter effects here, but we have checked that, in the parameter ranges of interest to us, the day-night effect caused by the earth matter is of the order of few per cent, comparable to the day-night effect in the Standard Model. We thus anticipate that our limits would only change marginally if Earth matter effects were included.

In order to verify that the assumption of full adiabaticity is justified, we have examined the adiabaticity parameter γ in the two flavour approximation and we have checked that the adiabaticity condition [35]

$$\gamma^{-1} = \frac{\sin 2\theta \frac{\Delta m^2_{ij}}{2E}}{|\lambda_i - \lambda_j|^3} \cdot \left| \frac{dV_b}{dt} \right| \ll 1 \tag{3.8}$$

holds for all relevant mass squared difference Δm^2_{ij} even for large V_b and the smallest relevant differences between the Hamiltonian eigenvalues λ_i and λ_j, which occur at the resonance position. We determine the derivative of the matter potential, $\left|dV_b/dt\right|$, from the solar density profile of the standard solar model BS'05 (OP) [52].

In figure 5, we compare the measured solar neutrino oscillation probabilities $P_{\nu_e \to \nu_e}$ to the theoretical predictions for standard three flavour oscillations and for the best fitting baryonic neutrino scenarios with $\epsilon > 0$ (blue) and $\epsilon < 0$ (red).

We observe that for $\epsilon < 0$, a peak-like structure appears in $P_{\nu_e \to \nu_e}$, which suggests that mixing of ν_e with other flavors is dynamically driven to zero for specific parameter combinations. The peak occurs at parameter points where $\Delta m^2_{41}/(2E),\ \Delta m^2_{31}/(2E) \gg \Delta m^2_{21}/(2E)$, V_b and where moreover θ_{34} and θ_{13} are small. To understand its origin, it is therefore helpful to determine the eigenvalues of the Hamiltonian $H^{\text{flavor}}_{\text{eff}}$ (see equation (2.10)) using time-independent perturbation theory, with the zeroth order Hamiltonian given by

$$H^{\text{flavour},(0)}_{\text{eff}} \equiv \frac{1}{2E} U \,\text{diag}(0, 0, \Delta m^2_{31}, \Delta m^2_{41}) U^\dagger \,, \tag{3.9}$$

JHEP12(2014)104

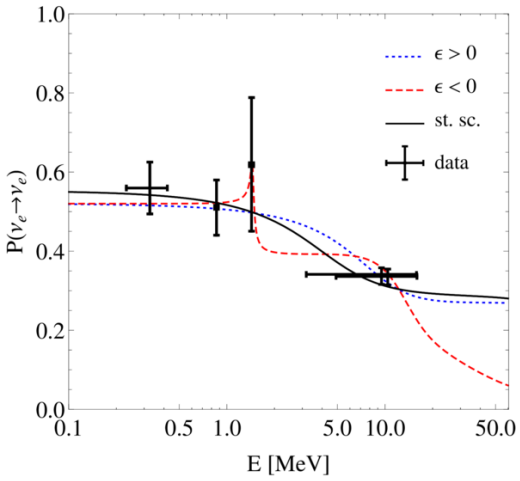

Figure 5. Comparison of the measured solar neutrino oscillation probabilities to our theoretical predictions for standard three flavour oscillations (black) and for the best fit parameter points of the baryonic sterile neutrino model with $\epsilon > 0$ (dotted blue) and $\epsilon < 0$ (dashed red).

and the perturbation being $H_{\text{eff}}^{\text{flavour},(1)} \equiv H_{\text{eff}}^{\text{flavour}} - H_{\text{eff}}^{\text{flavour},(0)}$. In the approximation $\theta_{34} = \theta_{13} = 0$, a set of zeroth order eigenvectors is obviously given by the matrix $U^{(0)} \equiv R'_{24}R'_{14}R_{23}$, where, as before, R_{ij} and R'_{ij} are real and complex rotation matrices, respectively. Since $H_{\text{eff}}^{\text{flavour},(0)}$ has zero as a double eigenvalue, we next have to find eigenvectors of $H_{\text{eff}}^{\text{flavour},(1)}$ in the subspace corresponding to this double eigenvalue. In other words, we need to compute $U^{(0)\dagger}H_{\text{eff}}^{\text{flavour},(1)}U^{(0)}$ and then diagonalize the upper left 2×2 block. It turns out that, if the condition

$$\frac{\Delta m^2_{21}}{2E} \sin 2\theta_{12} + V_b \cos\theta_{23} \sin\theta_{14} \sin 2\theta_{24} \simeq 0 \tag{3.10}$$

is fulfilled, this 2×2 block is automatically diagonal. This implies that $U^{(0)}(1,0,0,0)^T \simeq (1,0,0,0)$ is an approximate eigenvector of $H_{\text{eff}}^{\text{flavour}}$. Hence, if (3.10) holds at the center of the Sun, solar neutrinos are produced in an almost pure ν_1 mass eigenstate. After adiabatic flavour conversion, the resulting ν_e admixture is of order $\cos^2\theta_{12}$, leading to a peak in the observed solar neutrino spectrum at Earth.

3.2 Results

In figures 6 and 7 our constraints on the parameter space of baryonic sterile neutrinos are presented as contour plots for $\epsilon > 0$ and $\epsilon < 0$, respectively. We show exclusion limits (lines of constant $\chi^2 - \chi^2_{\text{min}}$) at the 95% and 3σ confidence levels. In each panel, we keep either ϵ or Δm^2_{41} fixed at the value indicated in the plot and show constraints on the remaining two parameters. Moreover, as discussed in section 3.1, we fixed $\sin^2 2\theta_{14} = 0.12$. Blue lines correspond to constraints from solar experiments, black lines are the limits from MINOS and the colored regions show the parameter region preferred by MiniBooNE. The best fit values for $\epsilon > 0$ and $\epsilon < 0$ are listed in table 2.

JHEP12(2014)104

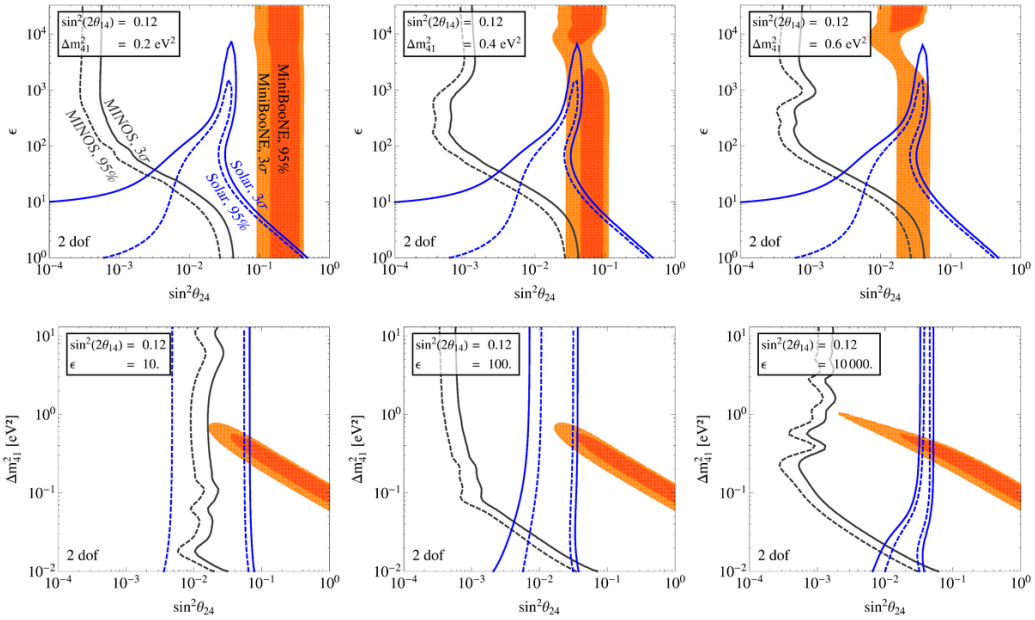

Figure 6. 95% and 3σ confidence level constraints on the parameters Δm^2_{41}, $\sin^2 2\theta_{24}$ and ϵ (strength of the new MSW potential) of the baryonic sterile neutrino model in the $\epsilon > 0$ case. Blue contours show constraints from solar experiments, black contours are for MINOS and shaded areas correspond to the region preferred by MiniBooNE. We have fixed $\sin^2 2\theta_{14} = 0.12$, as motivated by the reactor and gallium anomalies.

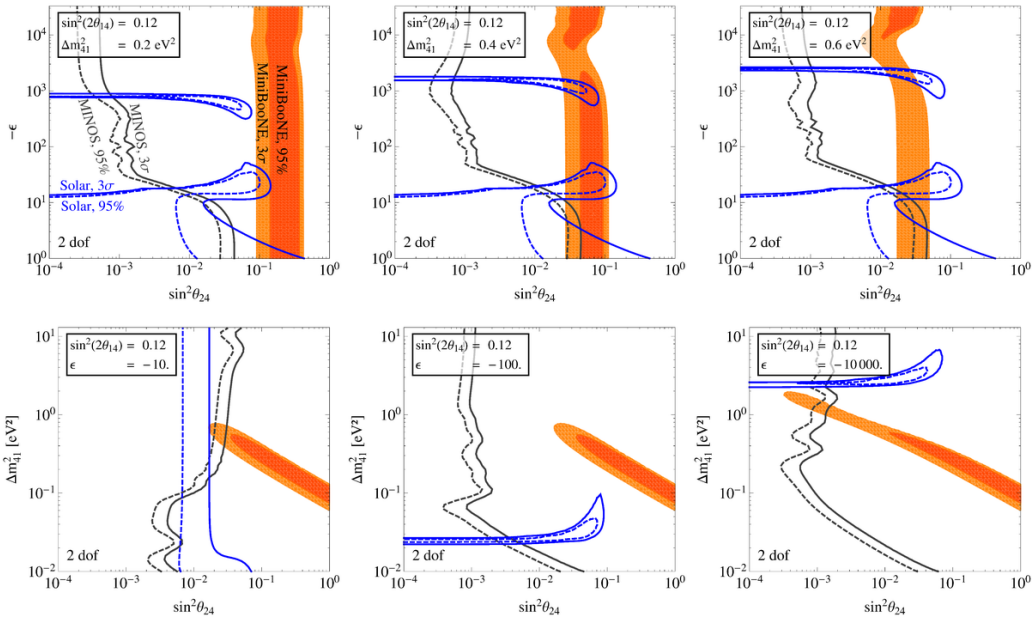

Figure 7. 95% and 3σ confidence level constraints on the parameters Δm^2_{41}, $\sin^2 2\theta_{24}$ and ϵ (strength of the new MSW potential) of the baryonic sterile neutrino model in the $\epsilon < 0$ case. Blue contours show constraints from solar experiments, black contours are for MINOS and shaded areas correspond to the region preferred by MiniBooNE. We have fixed $\sin^2 2\theta_{14} = 0.12$, as motivated by the reactor and gallium anomalies.

JHEP12(2014)104

		$\epsilon = G_B/(\sqrt{2}G_F)$	Δm^2_{41} [eV^2]	$\sin^2\theta_{24}$	$\chi^2_{\rm min}$/d.o.f.
MINOS	$\epsilon > 0$	16.9	0.014	0.0024	37.7/49
	$\epsilon < 0$	-19.2	0.037	0.00083	36.1/49
MiniBooNE	$\epsilon > 0$	30634	0.316	0.10	16.1/20
	$\epsilon < 0$	-32000	0.116	0.75	16.4/20
Solar	$\epsilon > 0$	0.20	insensitive	1.0	1.10/3
	$\epsilon < 0$	-38.0	0.013	0.046	0.41/3

Table 2. Best fit values resulting from our parameter scan for the different experimental data sets. For the MiniBooNE fit with $\epsilon < 0$ analysis the best fit value for ϵ is located outside the boundary of the analysis region, but χ^2 hardly depends on $|\epsilon|$ in this region. Also note that the solar best fit in the $\epsilon > 0$ case has $\epsilon < 1$ and is not sensitive to the exact value of Δm^2_{41} in the interval $[0.01, 11]$.

We see that values of $|\epsilon| \gtrsim 10$ are strongly disfavored by MINOS except in the case of tiny active-sterile mixing angles. For such large values of ϵ, the new MSW resonance at $\Delta m^2_{41}/(2E) \sim V_b$ lies within the MINOS energy range $E < 50\,\text{GeV}$ and leads to a constraint $\sin^2\theta_{24} \lesssim 10^{-3}$. Such small mixing angles are, however, irrelevant for possible explanations of MiniBooNE and other short-baseline anomalies. The MINOS contours also show that in most of the mass range $10^{-2}\ \text{eV}^2 \lesssim \Delta m^2_{41} \lesssim 10^{1}\ \text{eV}^2$, values of $\sin^2\theta_{24} \gtrsim 0.01$ are excluded, with limits becoming much stronger at large ϵ.

Solar neutrinos also have some sensitivity to θ_{24}, but limits on ϵ vary a lot with $\sin^2\theta_{24}$. For intermediate values $0.01 \lesssim \sin^2\theta_{24} \lesssim 0.1$, even values of $|\epsilon|$ as large as few $\times\, 10^3$ are compatible with solar neutrino data. For $\epsilon > 0$, we notice that solar limits on ϵ are weakest at $\sin^2\theta_{24} \sim$ few $\times\, 10^{-2}$. In this regime, the additional neutrino disappearance due to nonzero θ_{14} and θ_{24} is partially compensated by V_b-induced modifications to the MSW resonance structure. In particular, the 1–4 and 2–4 mixings imply that above the solar MSW resonance, ν_1–ν_2 mixing is not as strongly suppressed as in the standard case. This reduces the flavour transition probability at energies above the resonance. Note that this effect is related to a sterile neutrino-induced smearing of the *atmospheric* resonance (which at the center of the Sun lies at about 200 MeV) to the extent that it has a small impact even at energies as low as $\sim 10\,\text{MeV}$. The effect is therefore absent if the neutrino mass ordering is inverted so that the atmospheric resonance lies in the anti-neutrino sector. We have checked that indeed the limits on ϵ from solar neutrino experiments become somewhat weaker in this case. For $\epsilon < 0$, the exclusion contours reveal an allowed "island" at $\epsilon \sim -10^3$. In the parameter region corresponding to these islands, the non-standard MSW resonance at $\Delta m^2_{41}/2E \simeq V_b$ mimics the effect of the standard solar resonance. Note that such strong resonant conversion of active neutrinos into sterile neutrinos could have an observable impact on the SNO NC data, which is not included in our analysis because its impact is expected to be negligible in most of the parameter space (see section 3.1.3). Also, in this parameter region, the atmospheric MSW resonance — modified by the presence of the sterile neutrinos — has a small impact. Therefore, the "islands" move down by almost an order of magnitude in $|\epsilon|$ if the neutrino mass ordering is inverted. The Δm^2_{41}-independent "peninsula" at $\epsilon \sim -20$, is related to the appearance of the peak structure in $P_{\nu_e \to \nu_e}$ which we discussed in section 3.1.3 and which is independent of the mass ordering.

JHEP12(2014)104

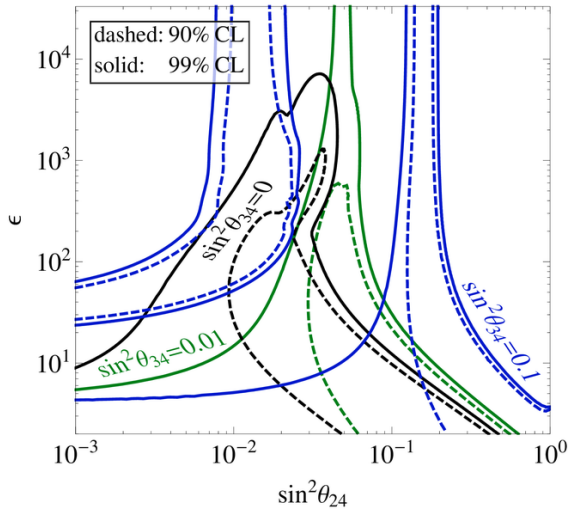

Figure 8. Constraints on ϵ and $\sin^2\theta_{24}$ from solar neutrinos for fixed $\sin^2 2\theta_{14} = 0.12$ (as motivated by the reactor and gallium anomalies), but for different values of θ_{34}. The value of Δm^2_{41} has been marginalized over in the range $10^{-2} \leq \Delta m^2_{41} \leq 1.1 \cdot 10^1$.

The allowed parameter region for the measured appearance signal in MiniBooNE is very similar to the one obtained in conventional sterile neutrino scenarios (see for instance the analysis by the MiniBooNE collaboration themselves [2]) with the exception that for large matter potentials, the allowed region is expanded towards lower $\sin^2\theta_{24}$ and higher Δm^2_{41}.

We now relax our assumption $\theta_{34} = 0$. The main sensitivity to θ_{34} is expected to come from solar neutrinos [15] (and from MINOS neutral current measurements, which we did not consider in this work, though). We compare the solar neutrino limits in the $\sin^2\theta_{24}$–ϵ plane for different values of θ_{34} in figure 8, marginalizing over the sterile neutrino mass in the range $10^{-2} \leq \Delta m^2_{41} \leq 1.1 \cdot 10^1$. We see that the constraints on ϵ become somewhat weaker if $\sin^2\theta_{34} \sim 0.01$ and change significantly for larger values of $\sin^2\theta_{34}$. This implies that, for large θ_{34}, a scenario with strong non-standard matter potential can be consistent with solar data and with MiniBooNE. Nevertheless, such a scenario would still be ruled out by MINOS.

Finally, let us also discuss the effect of choosing $\sin^2 2\theta_{14}$ different from the value 0.12 preferred by the reactor neutrino anomaly. To this end, we show in figure 9 how the constraints on ϵ and θ_{24} for fixed Δm^2_{41} are modified if $\sin^2 2\theta_{14}$ is taken a factor of 2 smaller (left panel) or a factor of 2 larger (right panel) than the preferred value. We see that the MiniBooNE preferred region, which is sensitive only to the combination $\sin^2 2\theta_{14} \sin^2\theta_{24}$ is simply shifted by a factor of 2. Solar limits are affected in a less trivial way and we find that at large θ_{14}, there is even a preference for nonzero θ_{24}. Note, however, that the goodness of fit becomes slightly worse as θ_{14} is increased: the minimum χ^2/dof is 0.8/3 for $\sin^2 2\theta_{14} = 0.6$ and 2.7/3 for $\sin^2 2\theta_{14} = 0.24$. Finally, MINOS limits are weakened if θ_{14} is large, especially at large ϵ. This happens because a larger mixing between ν_e and ν_b by unitarity implies more ν_μ disappearance.

JHEP12(2014)104

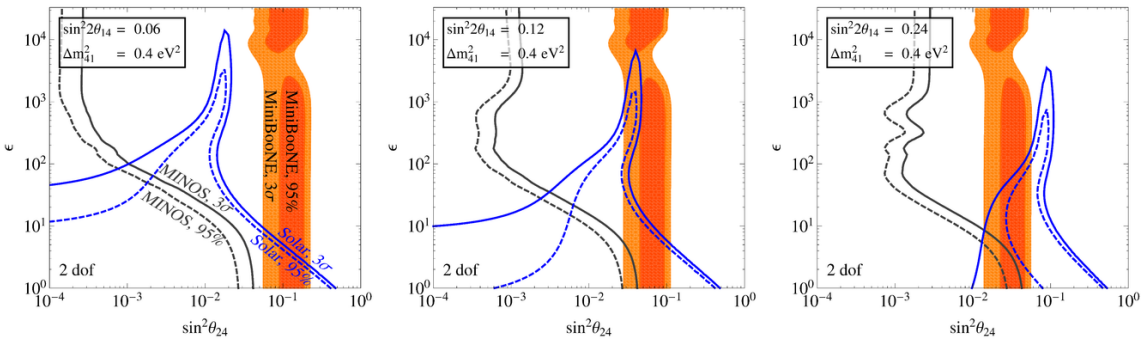

Figure 9. The effect of varying θ_{14} on the constraints in the $\sin^2\theta_{24}$–ϵ plane. The plot in the center reproduces middle panel in the upper row of figure 6, while the left and right panels show similar constraints for smaller and larger θ_{14}, respectively.

4 Conclusions

To summarize, we have derived constraints on models with extended sterile neutrino sectors that feature in particular a new gauge interaction between sterile neutrinos and SM particles. As a specific example, we have considered a scenario in which eV-scale sterile neutrinos are charged under gauged baryon number $\mathrm{U}(1)_B$. In principle, such interactions could be several orders of magnitude stronger than SM weak interactions, so the Mikheyev-Smirnov-Wolfenstein (MSW) potentials they generate could be significantly larger than the matter potential in standard three-flavour neutrino oscillations.

We have also computed approximate analytic expressions for the relevant oscillation probabilities in matter, improving and extending the expressions previously derived in [32]. We have then numerically analyzed data from the MINOS experiment, from solar neutrino measurements and from MiniBooNE to show that new gauge interactions in the sterile neutrino sector cannot be large unless the active-sterile neutrino mixing is very small. In particular, if the ratio ϵ of the non-standard and standard matter potentials is larger than $\sim$ 10, MINOS excludes mixing angles down to $\sin^2 2\theta_{24} \sim 10^{-3}$. (This limit becomes stronger if $\theta_{14} = 0$.)

We conclude that sterile neutrino searches in oscillation experiments are powerful tools to constrain certain models with hidden sector gauge interactions. We also conclude that such models do not help to resolve the tension in the global fit to short-baseline oscillation data.

Comparing to the interaction strength required for baryonic sterile neutrinos to yield signals in dark matter detectors [27–30], we conclude that in the case of eV scale sterile neutrinos, baryonic interactions cannot be large enough to be observable in the current generation of experiments. On the other hand, interesting signals may still be possible in future ton-scale experiments.

Acknowledgments

It is a pleasure to thank Janet Conrad and Georgia Karagiorgi for very helpful discussions.

JHEP12(2014)104

References

[1] LSND collaboration, A. Aguilar-Arevalo et al., *Evidence for neutrino oscillations from the observation of anti-neutrino(electron) appearance in a anti-neutrino(muon) beam*, *Phys. Rev.* **D 64** (2001) 112007 [hep-ex/0104049] [INSPIRE].

[2] MiniBooNE collaboration, A.A. Aguilar-Arevalo et al., *Improved Search for $\bar{\nu}_\mu \to \bar{\nu}_e$ Oscillations in the MiniBooNE Experiment*, *Phys. Rev. Lett.* **110** (2013) 161801 [arXiv:1207.4809] [INSPIRE].

[3] T. Mueller et al., *Improved Predictions of Reactor Antineutrino Spectra*, *Phys. Rev.* **C 83** (2011) 054615 [arXiv:1101.2663] [INSPIRE].

[4] G. Mention et al., *The Reactor Antineutrino Anomaly*, *Phys. Rev.* **D 83** (2011) 073006 [arXiv:1101.2755] [INSPIRE].

[5] P. Huber, *On the determination of anti-neutrino spectra from nuclear reactors*, *Phys. Rev.* **C 84** (2011) 024617 [*Erratum ibid.* **C 85** (2012) 029901] [arXiv:1106.0687] [INSPIRE].

[6] A.C. Hayes, J.L. Friar, G.T. Garvey, G. Jungman and G. Jonkmans, *Systematic Uncertainties in the Analysis of the Reactor Neutrino Anomaly*, *Phys. Rev. Lett.* **112** (2014) 202501 [arXiv:1309.4146] [INSPIRE].

[7] M.A. Acero, C. Giunti and M. Laveder, *Limits on ν_e and $\bar{\nu}_e$ disappearance from Gallium and reactor experiments*, *Phys. Rev.* **D 78** (2008) 073009 [arXiv:0711.4222] [INSPIRE].

[8] C. Giunti and M. Laveder, *Statistical Significance of the Gallium Anomaly*, *Phys. Rev.* **C 83** (2011) 065504 [arXiv:1006.3244] [INSPIRE].

[9] J. Kopp, M. Maltoni and T. Schwetz, *Are there sterile neutrinos at the eV scale?*, *Phys. Rev. Lett.* **107** (2011) 091801 [arXiv:1103.4570] [INSPIRE].

[10] C. Giunti and M. Laveder, *Implications of 3+1 Short-Baseline Neutrino Oscillations*, *Phys. Lett.* **B 706** (2011) 200 [arXiv:1111.1069] [INSPIRE].

[11] G. Karagiorgi, *Confronting Recent Neutrino Oscillation Data with Sterile Neutrinos*, arXiv:1110.3735 [INSPIRE].

[12] C. Giunti and M. Laveder, *Status of 3+1 Neutrino Mixing*, *Phys. Rev.* **D 84** (2011) 093006 [arXiv:1109.4033] [INSPIRE].

[13] C. Giunti and M. Laveder, *3+1 and 3+2 Sterile Neutrino Fits*, *Phys. Rev.* **D 84** (2011) 073008 [arXiv:1107.1452] [INSPIRE].

[14] K.N. Abazajian et al., *Light Sterile Neutrinos: A White Paper*, arXiv:1204.5379 [INSPIRE].

[15] J. Kopp, P.A.N. Machado, M. Maltoni and T. Schwetz, *Sterile Neutrino Oscillations: The Global Picture*, *JHEP* **05** (2013) 050 [arXiv:1303.3011] [INSPIRE].

[16] Planck collaboration, *Planck 2013 results. XVI. Cosmological parameters*, *Astron. Astrophys.* **571** (2014) A16 [arXiv:1303.5076] [INSPIRE].

JHEP12(2014)104

[17] BICEP2 collaboration, P.A.R. Ade et al., *Detection of B-Mode Polarization at Degree Angular Scales by BICEP2*, *Phys. Rev. Lett.* **112** (2014) 241101 [arXiv:1403.3985] [INSPIRE].

[18] E. Giusarma, E. Di Valentino, M. Lattanzi, A. Melchiorri and O. Mena, *Relic Neutrinos, thermal axions and cosmology in early 2014*, *Phys. Rev.* **D 90** (2014) 043507 [arXiv:1403.4852] [INSPIRE].

[19] C. Dvorkin, M. Wyman, D.H. Rudd and W. Hu, *Neutrinos help reconcile Planck measurements with both Early and Local Universe*, *Phys. Rev.* **D 90** (2014) 083503 [arXiv:1403.8049] [INSPIRE].

[20] H. Li, J.-Q. Xia and X. Zhang, *Global fitting analysis on cosmological models after BICEP2*, arXiv:1404.0238 [INSPIRE].

[21] J.-F. Zhang, Y.-H. Li and X. Zhang, *Sterile neutrinos help reconcile the observational results of primordial gravitational waves from Planck and BICEP2*, arXiv:1403.7028 [INSPIRE].

[22] M. Archidiacono et al., *Light sterile neutrinos after BICEP-2*, *JCAP* **06** (2014) 031 [arXiv:1404.1794] [INSPIRE].

[23] S. Hannestad, R.S. Hansen and T. Tram, *How Self-Interactions can Reconcile Sterile Neutrinos with Cosmology*, *Phys. Rev. Lett.* **112** (2014) 031802 [arXiv:1310.5926] [INSPIRE].

[24] B. Dasgupta and J. Kopp, *Cosmologically Safe eV-Scale Sterile Neutrinos and Improved Dark Matter Structure*, *Phys. Rev. Lett.* **112** (2014) 031803 [arXiv:1310.6337] [INSPIRE].

[25] T. Bringmann, J. Hasenkamp and J. Kersten, *Tight bonds between sterile neutrinos and dark matter*, *JCAP* **07** (2014) 042 [arXiv:1312.4947] [INSPIRE].

[26] P. Ko and Y. Tang, *$\nu\Lambda$MDM: A Model for Sterile Neutrino and Dark Matter Reconciles Cosmological and Neutrino Oscillation Data after BICEP2*, *Phys. Lett.* **B 739** (2014) 62 [arXiv:1404.0236] [INSPIRE].

[27] M. Pospelov, *Neutrino Physics with Dark Matter Experiments and the Signature of New Baryonic Neutral Currents*, *Phys. Rev.* **D 84** (2011) 085008 [arXiv:1103.3261] [INSPIRE].

[28] R. Harnik, J. Kopp and P.A.N. Machado, *Exploring nu Signals in Dark Matter Detectors*, *JCAP* **07** (2012) 026 [arXiv:1202.6073] [INSPIRE].

[29] M. Pospelov and J. Pradler, *Elastic scattering signals of solar neutrinos with enhanced baryonic currents*, *Phys. Rev.* **D 85** (2012) 113016 [arXiv:1203.0545] [INSPIRE].

[30] M. Pospelov and J. Pradler, *Dark Matter or Neutrino recoil? Interpretation of Recent Experimental Results*, *Phys. Rev.* **D 89** (2014) 055012 [arXiv:1311.5764] [INSPIRE].

[31] C.M. Ho and R.J. Scherrer, *Sterile Neutrinos and Light Dark Matter Save Each Other*, *Phys. Rev.* **D 87** (2013) 065016 [arXiv:1212.1689] [INSPIRE].

[32] G. Karagiorgi, M.H. Shaevitz and J.M. Conrad, *Confronting the Short-Baseline Oscillation Anomalies with a Single Sterile Neutrino and Non-Standard Matter Effects*, arXiv:1202.1024 [INSPIRE].

[33] P. Fileviez Perez and M.B. Wise, *Baryon and lepton number as local gauge symmetries*, *Phys. Rev.* **D 82** (2010) 011901 [*Erratum ibid.* **D 82** (2010) 079901] [arXiv:1002.1754] [INSPIRE].

[34] M. Duerr, P. Fileviez Perez and M.B. Wise, *Gauge Theory for Baryon and Lepton Numbers with Leptoquarks*, *Phys. Rev. Lett.* **110** (2013) 231801 [arXiv:1304.0576] [INSPIRE].

[35] E.K. Akhmedov, *Neutrino physics*, hep-ph/0001264 [INSPIRE].

JHEP12(2014)104

[36] C. Giunti and C.W. Kim, *Fundamentals of Neutrino Physics and Astrophysics*, Oxford University Press, Oxford, New York U.S.A. (2007).

[37] MiniBooNE collaboration, A.A. Aguilar-Arevalo et al., *A Search for electron neutrino appearance at the $\Delta m^2 \sim 1eV^2$ scale*, *Phys. Rev. Lett.* **98** (2007) 231801 [arXiv:0704.1500] [INSPIRE].

[38] MiniBooNE collaboration, A.A. Aguilar-Arevalo et al., *A Search for Electron Antineutrino Appearance at the $\Delta m^2 \sim 1$ eV^2 Scale*, *Phys. Rev. Lett.* **103** (2009) 111801 [arXiv:0904.1958] [INSPIRE].

[39] MiniBooNE collaboration, A.A. Aguilar-Arevalo et al., *Event Excess in the MiniBooNE Search for $\bar{\nu}_\mu \to \bar{\nu}_e$ Oscillations*, *Phys. Rev. Lett.* **105** (2010) 181801 [arXiv:1007.1150] [INSPIRE].

[40] P. Huber, J. Kopp, M. Lindner, M. Rolinec and W. Winter, *Globes manual* (2013), http://www.mpi-hd.mpg.de/personalhomes/globes/documentation/globes-manual-3.0.8.pdf.

[41] M. Beuthe, *Oscillations of neutrinos and mesons in quantum field theory*, *Phys. Rept.* **375** (2003) 105 [hep-ph/0109119] [INSPIRE].

[42] M.C. Gonzalez-Garcia, M. Maltoni, J. Salvado and T. Schwetz, *Global fit to three neutrino mixing: critical look at present precision*, *JHEP* **12** (2012) 123 [arXiv:1209.3023] [INSPIRE].

[43] P. Huber, M. Lindner and W. Winter, *Simulation of long-baseline neutrino oscillation experiments with GLoBES (General Long Baseline Experiment Simulator)*, *Comput. Phys. Commun.* **167** (2005) 195 [hep-ph/0407333] [INSPIRE].

[44] P. Huber, J. Kopp, M. Lindner, M. Rolinec and W. Winter, *New features in the simulation of neutrino oscillation experiments with GLoBES 3.0: General Long Baseline Experiment Simulator*, *Comput. Phys. Commun.* **177** (2007) 432 [hep-ph/0701187] [INSPIRE].

[45] MINOS collaboration, D.G. Michael et al., *Observation of muon neutrino disappearance with the MINOS detectors and the NuMI neutrino beam*, *Phys. Rev. Lett.* **97** (2006) 191801 [hep-ex/0607088] [INSPIRE].

[46] D. Anderson, *Theory of the Earth*, Blackwell Scientific Publications (1989) [ISBN 978-0-865-42123-3].

[47] M. Diwan et al., *Ion Chambers for Monitoring the NuMI Beam at FNAL*, in Proc. *9th European Particle Accelerator Conference (EPAC)*, Lucerne, Switzerland (2004).

[48] MINOS collaboration, J. de Jong, *Near-to-Final MINOS Oscillation Results*, *Nucl. Phys. Proc. Suppl.* **237-238** (2013) 166.

[49] MINOS collaboration, P. Adamson et al., *Measurement of Neutrino and Antineutrino Oscillations Using Beam and Atmospheric Data in MINOS*, *Phys. Rev. Lett.* **110** (2013) 251801 [arXiv:1304.6335] [INSPIRE].

[50] MiniBooNE collaboration, A.A. Aguilar-Arevalo et al., *Improved Search for $\bar{\nu}_\mu \to \bar{\nu}_e$ Oscillations in the MiniBooNE Experiment*, *Phys. Rev. Lett.* **110** (2013) 161801 [arXiv:1207.4809] [INSPIRE].

[51] Borexino collaboration, G. Bellini et al., *Final results of Borexino Phase-I on low energy solar neutrino spectroscopy*, *Phys. Rev.* **D 89** (2014) 112007 [arXiv:1308.0443] [INSPIRE].

[52] J.N. Bahcall, A.M. Serenelli and S. Basu, *New solar opacities, abundances, helioseismology and neutrino fluxes*, *Astrophys. J.* **621** (2005) L85 [astro-ph/0412440] [INSPIRE].

JHEP12(2014)104